Study of double-charm and double-strange tetraquark $X_{cc\bar{s}\bar{s}}$

Yuheng Wu,[1,*] Xin Jin,[1,†] Runxin Liu,[1,‡] Xinmei Zhu,[2,§] Hongxia Huang,[1,‖] and Jialun Ping[1,¶]
[1]Department of Physics, Nanjing Normal University, Nanjing, Jiangsu 210097, China
[2]Department of Physics, Yangzhou University, Yangzhou 225009, People's Republic of China

(Received 26 December 2021; revised 10 April 2023; accepted 24 April 2023; published 9 May 2023)

In the framework of the quark delocalization color screening model, we search for the double-charm and double-strange tetraquark $X_{cc\bar{s}\bar{s}}$ with two structures: $Q\bar{q}-Q\bar{q}$ and $QQ-\bar{q}\,\bar{q}$. The bound-state calculation shows that there is no bound state in the present work. However, by applying a stabilization calculation and coupling all channels of both structures, two new resonance states with $IJ^P = 00^+$ are obtained, one with mass and width around 4250 and 6 MeV, respectively, and another one with mass and width around 4300 and 19 MeV, respectively. Both of these states are more likely to be the compact resonance states. Although no significant signals were observed in the present experiment at the Belle Collaboration, there are still some structures around 4.3 GeV in the distributions of $M_{D_s^+D_s^+}$ and $M_{D_s^{*+}D_s^{*+}}$. We suggest that the experiment can be further tested with a larger amount of data.

DOI: 10.1103/PhysRevD.107.094011

I. INTRODUCTION

Over the past decades, dozens of exotic hadron states have been reported in experiments worldwide. These states provide us with an ideal platform to deepen our understanding of nonperturbative quantum chromodynamics (QCD). Although none of the exotic states is now definitely confirmed by experiment, more and more theoretical work has been done to investigate the exotic states. Searching for new exotic states is one of the most significant research topics in hadron physics.

The hidden-charm and hidden-strange tetraquark, which is composed of $cs\bar{c}\,\bar{s}$, is one type of exotic states. In 2009, the CDF Collaboration reported the $X(4140)$ in the $J/\psi\phi$ invariant mass distribution [1]. Later, the $X(4140)$ was successively observed by other experiments, such as the Belle [2], CMS [3], D0 [4], *BABAR* [5], and LHCb [6] Collaborations. In 2010, a narrow resonance $X(4350)$ was observed in the $\gamma\gamma \to J/\psi\phi$ process by the Belle Collaboration [2]. In 2016, the LHCb Collaboration reported four exotic states $X(4140)$, $X(4274)$, $X(4500)$, and $X(4700)$ from the amplitude analysis of the $B^+ \to J/\psi\phi K^+$ decays [7,8]. In 2017, the $X(4274)$ was reported by the CDF Collaboration in the process of $B^+ \to J/\psi\phi K^+$ [9]. In 2020, the LHCb Collaboration reported a new state $\chi_{c0}(3930)$, which is just below the $D_s^-D_s^+$ threshold [10,11]. In 2021, two new hadron states $X(4685)$ and $X(4630)$ were reported with the help of the improved full amplitude analysis of the $B^+ \to J/\psi\phi K^+$ decay by the LHCb Collaboration [12].

These experimental developments aroused great interest in studying the hidden-charm and hidden-strange tetraquarks. In Ref. [13], Liu *et al.* investigated the tetraquark composed of $cs\bar{c}\bar{s}$ and found that the $X(4350)$, $X(4500)$, and $X(4700)$ could be explained as the compact tetraquarks with $IJ^P = 00^+$ and the $X(4274)$ was explained as a compact tetraquark with $IJ = 01^+$. In the framework of the chiral quark model, Yang and Ping found that the $X(4274)$ could be the $cs\bar{c}\bar{s}$ tetraquark with $J^{PC} = 1^{++}$ and the $X(4350)$ could be assigned as a candidate of the compact tetraquark with $J^{PC} = 0^{++}$. For the $X(4700)$, it is explained as the $2S$ radial excited tetraquark with $J^{PC} = 0^{++}$ [14]. In Ref. [15], the $cs\bar{c}\,\bar{s}$ tetraquarks were studied within the $QQ-\bar{q}\bar{q}$ configuration by using the QCD sum rule. They claimed that the $X(4140)$ and $X(4274)$ could be assigned as the S-wave $cs\bar{c}\,\bar{s}$ tetraquarks with opposite color structures and both the $X(4500)$ and $X(4700)$ were the D-wave $cs\bar{c}\bar{s}$ tetraquarks with opposite color structures, too. More results and discussions are given in Refs. [16–22].

Recently, the BESIII Collaboration reported a new structure $Z_{cs}(3985)^-$ near the $D_s^-D^{*0}/D_s^{*-}D^0$ thresholds

*191002007@njnu.edu.cn
†181002005@njnu.edu.cn
‡201002011@njnu.edu.cn
§xmzhu@yzu.edu.cn
‖Corresponding author.
hxhuang@njnu.edu.cn
¶Corresponding author.
jlping@njnu.edu.cn

Published by the American Physical Society under the terms of the Creative Commons Attribution 4.0 International license. Further distribution of this work must maintain attribution to the author(s) and the published article's title, journal citation, and DOI. Funded by SCOAP³.

in the processes of $e^+e^- \to K^+(D_s^- D^{*0} + D_s^{*-} D^0)$. The mass and width of this state are $(3982.5^{+1.8}_{-2.6} \pm 2.1)$ and $(12.8^{+5.3}_{-4.4} \pm 3.0)$ MeV, respectively [23]. From the production mode, the minimum quark component of $Z_{cs}(3985)^-$ is $cs\bar{c}\,\bar{u}$, so it is the first candidate of the charged hidden-charm tetraquark state with strangeness. Later, the LHCb Collaboration reported two new states $Z_{cs}(4000)^+$ and $Z_{cs}(4220)^+$ with the quark content of $cu\bar{c}\bar{s}$ decaying to the $J/\psi K^+$ [12]. The decay widths of these two states are $\Gamma = 131 \pm 15 \pm 26$ MeV and $\Gamma = 233 \pm 52^{+97}_{-73}$ MeV, respectively. Obviously, the masses of $Z_{cs}(3985)^-$ and $Z_{cs}(4000)^+$ are close, but the decay widths are largely different. These observations immediately stimulated a lot of theoretical studies of the open-strange and hidden-charm tetraquarks [24–39]. Some works showed that $Z_{cs}(3985)^-$ and $Z_{cs}(4000)^+$ are the same state [40,41], while some indicated that they are not the same state [29,42–44].

Inspired by the study progress of the hidden-charm and hidden-strange tetraquarks and the open-strange and hidden-charm tetraquarks, it is natural to investigate the existence of the open-charm and open-strange tetraquarks. Very recently, the Belle Collaboration searched for the double-heavy tetraquark state candidates $X_{cc\bar{s}\bar{s}}$ decaying to $D_s^+ D_s^+$ and $D_s^{*+} D_s^{*+}$, but no significant signals were observed [45]. In Ref. [46], the double-charm and double-strange tetraquarks $cc\bar{s}\bar{s}$ were studied within the chiral quark model, and some resonance states with $IJ^P = 00^+$ and 02^+ were obtained. In Ref. [47], the $D_s^{*+} D_s^{*+}$ systems with $IJ^P = 00^+$ and 02^+ were studied in a coupled channel unitary approach, but no bound state was found because of the strong repulsion.

As is commonly believed, QCD is the fundamental theory of the strong interaction. However, the low-energy physics of QCD, such as hadron structure, hadron-hadron interactions, and the structure of multiquark systems, is much harder to calculate directly from QCD. The quark delocalization color screening model (QDCSM), which was developed in the 1990s with the aim of explaining the similarities between nuclear and molecular forces [48], is one of the effective approaches for studying multiquark systems. Two new ingredients were introduced: quark delocalization (to enlarge the model variational space to take into account the mutual distortion or the internal excitations of nucleons in the course of their interactions, the distortion of wave functions in the existence of other nucleons is also considered in the quark-meson-coupling model [49]) and color screening (assuming the quark-quark interaction dependent on quark states aimed to take into account the QCD effect which has not yet been included in the two-body confinement and effective one-gluon exchange). This model has been applied to the study of the dibaryons [50,51], pentaquarks [52,53] and some tetraquark systems [13]. It is also interesting to extend this model to study the open-charm and open-strange tetraquarks. As the first step, we investigate the existence of the double-charm and double-strange tetraquarks $cc\bar{s}\,\bar{s}$ in this work. Different structures and the effect of channel coupling are considered.

The structure of this paper is as follows. Section II gives a brief description of the quark model and wave functions. Section III is devoted to the numerical results and discussions. The summary is shown in the last section.

II. MODEL AND WAVE FUNCTIONS

A. The QDCSM

In this paper, we use the QDCSM to investigate the $cc\bar{s}\,\bar{s}$ tetraquark system. The details of the QDCSM can be found in Refs. [48,50,51]. Here, we just present the Hamiltonian of the model:

$$H = \sum_{i=1}^{4}\left(m_i + \frac{p_i^2}{2m_i}\right) - T_{\rm CM} + \sum_{j>i=1}^{4}(V_{ij}^{\rm CON} + V_{ij}^{\rm OGE} + V_{ij}^{\rm OBE}), \quad (1)$$

$$V_{ij}^{\rm CON} = \begin{cases} -a_c \boldsymbol{\lambda}_i^c \cdot \boldsymbol{\lambda}_j^c (r_{ij}^2 + a_{ij}^0), & \text{if } i,j \text{ in the same cluster,} \\ -a_c \boldsymbol{\lambda}_i^c \cdot \boldsymbol{\lambda}_j^c \left(\frac{1-e^{-\mu_{ij} r_{ij}^2}}{\mu_{ij}} + a_{ij}^0\right), & \text{otherwise,} \end{cases} \quad (2)$$

$$V_{ij}^{\rm OGE} = \frac{1}{4}\alpha_s \boldsymbol{\lambda}_i^c \cdot \boldsymbol{\lambda}_j^c \left[\frac{1}{r_{ij}} - \frac{\pi}{2}\delta(r_{ij})\left(\frac{1}{m_i^2} + \frac{1}{m_j^2} + \frac{4\boldsymbol{\sigma}_i \cdot \boldsymbol{\sigma}_j}{3m_i m_j}\right)\right], \quad (3)$$

$$V_{ij}^{\rm OBE} = V_\eta(r_{ij})[(\lambda_i^8 \cdot \lambda_j^8)\cos\theta_P - (\lambda_i^0 \cdot \lambda_j^0)\sin\theta_P], \quad (4)$$

$$V_\eta(\boldsymbol{r}_{ij}) = \frac{g_{ch}^2}{4\pi}\frac{m_\eta^2}{12 m_i m_j}\frac{\Lambda_\eta^2}{\Lambda_\eta^2 - m_\eta^2} m_\eta \times \left\{(\boldsymbol{\sigma}_i \cdot \boldsymbol{\sigma}_j)\left[Y(m_\eta r_{ij}) - \frac{\Lambda_\eta^3}{m_\eta^3} Y(\Lambda_\eta r_{ij})\right]\right\}, \quad (5)$$

where $T_{\rm CM}$ is the kinetic energy of the center of mass; $V_{ij}^{\rm CON}$ and $V_{ij}^{\rm OGE}$ are the confinement and one-gluon-exchange

interactions, respectively; and $V_{ij}^{\rm OBE}$ is the Goldstone-boson exchange interaction. In Eq. (2), the μ_{ij} is the color screening parameter, which is determined by fitting the deuteron properties, NN scattering phase shifts, and $N\Lambda$ and $N\Sigma$ scattering phase shifts, with $\mu_{uu} = 0.45$ fm^{-2}, $\mu_{us} = 0.19$ fm^{-2}, and $\mu_{ss} = 0.08$ fm^{-2}, satisfying the relation $\mu_{us}^2 = \mu_{uu}\mu_{ss}$. When extending to the heavy-quark sector, we found that the dependence of the parameter μ_{cc} is not very significant in the calculation of the P_c states [52] by taking it from 0.0001 to 0.01 fm^{-2}. So here we take $\mu_{cc} = 0.01$ fm^{-2}. Then μ_{sc} and μ_{uc} are obtained by the relation $\mu^2 = \mu_{ss}\mu_{cc}$ and $\mu^2 = \mu_{uu}\mu_{cc}$, respectively. Here, we focus on the S-wave $cc\bar{s}\,\bar{s}$ states, so the tensor force interaction is not included. The $V_{ij}^{\rm OGE}$ can be briefly written as Eq. (3), where the α_s is the quark-gluon coupling constant. For the $V_{ij}^{\rm OBE}$, there are no π and K meson exchanges in the $cc\bar{s}\,\bar{s}$ system. So, we use only the η exchange here. In Eq. (5), the $Y(x) = e^{-x}/x$ is the standard Yukawa function; g_{ch} is the coupling constant for chiral field, which is determined from the $NN\pi$ coupling constant through

$$\frac{g_{ch}^2}{4\pi} = \left(\frac{3}{5}\right)^2 \frac{g_{\pi NN}^2}{4\pi}\frac{m_{u,d}^2}{m_N^2}. \tag{6}$$

The other symbols in the above expressions have their usual meanings. All model parameters, which are determined by fitting the meson spectrum, are from the work of the $c\bar{c}s\bar{s}$ system [13].

B. Wave function

The resonating group method (RGM) [54], a well-established method for studying a bound state or a scattering problem, is used to calculate the energy of all these states in this work. The wave function of the four-quark system is of the form

$$\Psi_{4q} = \mathcal{A}[[\Psi_A\Psi_B]^{[\sigma]IS} \otimes \chi(\mathbf{R})]^J. \tag{7}$$

The symbol $\mathcal{A}$ is the antisymmetrization operator. For the $cc\bar{s}\,\bar{s}$ system, we label two c quarks as quarks 1 and 3 and two $\bar{s}$ as 2 and 4. Then, $\mathcal{A} = 1 - P_{13} - P_{24} + P_{13}P_{24}$. $[\sigma] = [222]$ gives the total color symmetry, except that all other symbols have the usual meanings. Ψ_A and Ψ_B are the two-quark cluster wave functions:

$$\Psi_A = \left(\frac{1}{2\pi b^2}\right)^{3/4} e^{-\boldsymbol{\rho}_A^2/(4b^2)}\eta_{I_AS_A}\chi_A^c, \tag{8}$$

$$\Psi_B = \left(\frac{1}{2\pi b^2}\right)^{3/4} e^{-\boldsymbol{\rho}_B^2/(4b^2)}\eta_{I_BS_B}\chi_B^c, \tag{9}$$

where $\eta_{I_AS_A}$ ($\eta_{I_BS_B}$) represent the multiplied wave functions of flavor and spin of cluster A (B). χ_A^c (χ_B^c) are the internal color wave functions of cluster A (B). Different Jacobi coordinates are defined for different structures. For the meson-meson configuration ($c\bar{s} - c\bar{s}$), the Jacobi coordinates are defined as

$$\begin{aligned}
&\boldsymbol{\rho}_A = \mathbf{r}_1 - \mathbf{r}_2, \qquad \boldsymbol{\rho}_B = \mathbf{r}_3 - \mathbf{r}_4,\\
&\mathbf{R}_A = \frac{m_1\mathbf{r}_1 + m_2\mathbf{r}_2}{m_1 + m_2}, \qquad \mathbf{R}_B = \frac{m_3\mathbf{r}_3 + m_4\mathbf{r}_4}{m_3 + m_4},\\
&\mathbf{R} = \mathbf{R}_A - \mathbf{R}_B,\\
&\mathbf{R}_C = \frac{m_1\mathbf{r}_1 + m_2\mathbf{r}_2 + m_3\mathbf{r}_3 + m_4\mathbf{r}_4}{m_1 + m_2 + m_3 + m_4}.
\end{aligned} \tag{10}$$

For the diquark-antidiquark configuration ($cc - \bar{s}\,\bar{s}$), the Jacobi coordinates are defined as

$$\begin{aligned}
&\boldsymbol{\rho}_A = \mathbf{r}_1 - \mathbf{r}_3, \qquad \boldsymbol{\rho}_B = \mathbf{r}_2 - \mathbf{r}_4,\\
&\mathbf{R}_A = \frac{m_1\mathbf{r}_1 + m_3\mathbf{r}_3}{m_1 + m_3}, \qquad \mathbf{R}_B = \frac{m_2\mathbf{r}_2 + m_4\mathbf{r}_4}{m_2 + m_4},\\
&\mathbf{R} = \mathbf{R}_A - \mathbf{R}_B,\\
&\mathbf{R}_C = \frac{m_1\mathbf{r}_1 + m_2\mathbf{r}_2 + m_3\mathbf{r}_3 + m_4\mathbf{r}_4}{m_1 + m_2 + m_3 + m_4},
\end{aligned} \tag{11}$$

From the variational principle, after variation with respect to the relative motion wave function $\chi(\mathbf{R}) = \sum_L \chi_L(\mathbf{R})$, one obtains the RGM equation

$$\int H(\mathbf{R},\mathbf{R}')\chi(\mathbf{R}')d\mathbf{R}' = E\int N(\mathbf{R},\mathbf{R}')\chi(\mathbf{R}')d\mathbf{R}', \tag{12}$$

where $H(\mathbf{R},\mathbf{R}')$ and $N(\mathbf{R},\mathbf{R}')$ are the Hamiltonian and norm kernels, respectively. By solving the RGM equation, we can get the energies E and the wave functions. In fact, it is not convenient to work with the RGM expressions. Then, we use the Gaussian bases to expand the relative motion wave function $\chi(\mathbf{R})$, respectively:

$$\begin{aligned}
\chi(\boldsymbol{R}) = &\frac{1}{\sqrt{4\pi}}\left(\frac{1}{\pi b^2}\right)^{\frac{3}{4}}\sum_{i,L,M} C_{i,L}\\
&\times\int e^{-\frac{1}{2b^2}(\boldsymbol{R}-\boldsymbol{S}_i)^2} Y_{LM}(\hat{\boldsymbol{S}}_i)d\hat{\boldsymbol{S}}_i,
\end{aligned} \tag{13}$$

where $\boldsymbol{S_i}$ is the separation of two reference centers and plays the role of the generator coordinate in the model; $C_{i,L}$ is the expansion coefficient. After the inclusion of the center of mass motion,

$$\Phi_C(\boldsymbol{R}_C) = \left(\frac{4}{\pi b^2}\right)^{3/4} e^{-\frac{2\boldsymbol{R}_C^2}{b^2}}, \tag{14}$$

the ansatz [Eq. (7)] can be rewritten as

$$\Psi_{4q} = \mathcal{A}\sum_{i,L,M} C_{i,L} \int \frac{d\Omega_{S_i}}{\sqrt{4\pi}} \prod_{\alpha=1}^{2} \phi_\alpha(\boldsymbol{S_i}) \prod_{\beta=3}^{4} \phi_\beta(-\boldsymbol{S_i}) \times [[\eta_{I_A S_A}\eta_{I_B S_B}]^{IS} Y_{LM}(\boldsymbol{S_i})]^{J} [\chi_A^c \chi_B^c]^{[\sigma]}, \quad (15)$$

where $\phi_\alpha(\boldsymbol{S_i})$ and $\phi_\beta(-\boldsymbol{S_i})$ are the single-particle orbital wave functions with different reference centers:

$$\phi_\alpha(\boldsymbol{S_i}) = \left(\frac{1}{\pi b^2}\right)^{3/4} e^{-\frac{1}{2b^2}\left(\boldsymbol{r}_\alpha - \frac{\mu_{AB}}{M_A}\boldsymbol{S_i}\right)^2},$$
$$\phi_\beta(-\boldsymbol{S_i}) = \left(\frac{1}{\pi b^2}\right)^{3/4} e^{-\frac{1}{2b^2}\left(\boldsymbol{r}_\beta + \frac{\mu_{AB}}{M_B}\boldsymbol{S_i}\right)^2}. \quad (16)$$

Here, $\mu_{AB} = \frac{M_A M_B}{M_A + M_B}$; $M_A = m_1 + m_2$ and $M_B = m_3 + m_4$ for the $c\bar{s} - c\bar{s}$ structure, and $M_A = m_1 + m_3$ and $M_B = m_2 + m_4$ for the $cc - \bar{s}\,\bar{s}$ structure. With the reformulated ansatz [Eq. (15)], the RGM equation (12) becomes an algebraic eigenvalue equation:

$$\sum_{j,L} C_{j,L} H_{i,j}^{L,L'} = E \sum_{j} C_{j,L'} N_{i,j}^{L'}, \quad (17)$$

where $H_{i,j}^{L,L'}$ and $N_{i,j}^{L'}$ are the Hamiltonian matrix elements and overlaps (without the summation over L'), respectively. By solving the generalized eigenproblem, we can obtain the energies of the four-quark systems E and corresponding expansion coefficient $C_{j,L}$. Finally, the relative motion wave function between two clusters can be obtained by substituting $C_{j,L}$ into Eq. (13). Besides, the overlaps and Hamiltonian matrix elements can be used to calculate the effective potential. The effective potential between two mesons is defined as $V(S_i) = E(S_i) - E(\infty)$, where $E(S_i)$ is the energy of the system with the separation S_i of two reference centers, and $E(S_i) = H_{i,i}/N_{i,i}$, where $N_{i,i}$ and $H_{i,i}$ are overlaps and Hamiltonian matrix elements with the separation S_i, respectively.

In QDCSM, the quark delocalization is achieved by writing the single-particle orbital wave function as a linear combination of the left and right Gaussian functions, the single-particle orbital wave functions used in the ordinary quark cluster model:

$$\psi_\alpha(\mathbf{S}_i, \epsilon(\mathbf{S}_i)) = (\phi_\alpha(\mathbf{S}_i) + \epsilon(\mathbf{S}_i)\phi_\alpha(-\mathbf{S}_i))/N(\epsilon(\mathbf{S}_i)),$$
$$\psi_\beta(-\mathbf{S}_i, \epsilon(\mathbf{S}_i)) = (\phi_\beta(-\mathbf{S}_i) + \epsilon(\mathbf{S}_i)\phi_\beta(\mathbf{S}_i))/N(\epsilon(\mathbf{S}_i)),$$
$$N(\epsilon(\mathbf{S}_i)) = \sqrt{1 + \epsilon^2(\mathbf{S}_i) + 2\epsilon(\mathbf{S}_i)e^{-s_i^2/4b^2}}. \quad (18)$$

The $\epsilon(\mathbf{S}_i)$ is determined variationally by the dynamics of the multiquark system itself rather than an adjustable one, which can make the system choose the favorable configuration in the interacting process.

The flavor, spin, and color wave functions are constructed in the following part. In this work, the flavor wave function for the tetraquark system we investigate is $cc\bar{s}\,\bar{s}$. Different structures are obtained according to different coupling sequences. For the $Q\bar{q} - Q\bar{q}$ structure, the coupling sequence is

$$\chi_m^{f1} = c\bar{s} - c\bar{s}. \quad (19)$$

For the $QQ - \bar{q}\,\bar{q}$ structure, the coupling sequence is

$$\chi_d^{f1} = cc - \bar{s}\,\bar{s}\,. \quad (20)$$

For the spin wave functions of the $Q\bar{q} - Q\bar{q}$ structure, first, we construct the two-body spin wave functions as

$$\chi_{\sigma_{11}}^1 = \alpha\alpha, \qquad \chi_{\sigma_{10}}^2 = \sqrt{\frac{1}{2}}(\alpha\beta + \beta\alpha),$$
$$\chi_{\sigma_{1-1}}^3 = \beta\beta, \qquad \chi_{\sigma_{00}}^4 = \sqrt{\frac{1}{2}}(\alpha\beta - \beta\alpha). \quad (21)$$

Then the spin wave functions of the $Q\bar{q} - Q\bar{q}$ structure can be obtained by coupling the wave functions of two clusters:

$$\psi_0^1 = \chi_{\sigma_{00}}^4 \chi_{\sigma_{00}}^4,$$
$$\psi_0^2 = \sqrt{\frac{1}{3}}\left(\chi_{\sigma_{11}}^1 \chi_{\sigma_{1-1}}^3 - \chi_{\sigma_{10}}^2 \chi_{\sigma_{10}}^2 + \chi_{\sigma_{1-1}}^3 \chi_{\sigma_{11}}^1\right),$$
$$\psi_1^3 = \chi_{\sigma_{00}}^4 \chi_{\sigma_{11}}^1,$$
$$\psi_1^4 = \chi_{\sigma_{11}}^1 \chi_{\sigma_{00}}^4,$$
$$\psi_1^5 = \sqrt{\frac{1}{2}}\left(\chi_{\sigma_{11}}^1 \chi_{\sigma_{10}}^2 - \chi_{\sigma_{10}}^2 \chi_{\sigma_{11}}^1\right),$$
$$\psi_1^6 = \chi_{\sigma_{11}}^1 \chi_{\sigma_{11}}^1. \quad (22)$$

For the $QQ - \bar{q}\,\bar{q}$ structure, the spin wave functions are the same as the $Q\bar{q} - Q\bar{q}$ structure.

Finally, for the color wave function, the two structures are much different. The color wave function for a $Q\bar{q}$ cluster is

$$\chi_{[111]}^1 = \sqrt{\frac{1}{3}}(r\bar{r} + g\bar{g} + b\bar{b}). \quad (23)$$

Then the color wave function for the $Q\bar{q} - Q\bar{q}$ structure is

$$\psi^{c_1} = \chi_{[111]}^1 \chi_{[111]}^1. \quad (24)$$

However, the situation is even more complicated for the $QQ - \bar{q}\bar{q}$ structure. We construct the color wave function for the QQ and $\bar{q}\bar{q}$ clusters first. The color wave functions of the QQ clusters are

$$\chi^1_{[2]} = rr, \qquad \chi^2_{[2]} = \frac{1}{\sqrt{2}}(rg+gr), \qquad \chi^3_{[2]} = gg,$$
$$\chi^4_{[2]} = \frac{1}{\sqrt{2}}(rb+br), \qquad \chi^5_{[2]} = \frac{1}{\sqrt{2}}(gb+bg),$$
$$\chi^6_{[2]} = bb, \qquad \chi^7_{[11]} = \frac{1}{\sqrt{2}}(rg-gr),$$
$$\chi^8_{[11]} = \frac{1}{\sqrt{2}}(rb-br), \qquad \chi^9_{[11]} = \frac{1}{\sqrt{2}}(gb-bg), \tag{25}$$

and the color wave functions of the $\bar{q}\,\bar{q}$ clusters are

$$\chi^1_{[22]} = \bar{r}\,\bar{r}, \qquad \chi^2_{[22]} = -\frac{1}{\sqrt{2}}(\bar{r}\,\bar{g}+\bar{g}\,\bar{r}), \qquad \chi^3_{[22]} = \bar{g}\,\bar{g},$$
$$\chi^4_{[22]} = \frac{1}{\sqrt{22}}(\bar{r}\,\bar{b}+\bar{b}\,\bar{r}), \qquad \chi^5_{[22]} = -\frac{1}{\sqrt{2}}(\bar{g}\,\bar{b}+\bar{b}\,\bar{g}),$$
$$\chi^6_{[22]} = \bar{b}\,\bar{b}, \qquad \chi^7_{[211]} = \frac{1}{\sqrt{2}}(\bar{r}\,\bar{g}-\bar{g}\,\bar{r}),$$
$$\chi^8_{[211]} = -\frac{1}{\sqrt{2}}(\bar{r}\,\bar{b}-\bar{b}\,\bar{r}), \qquad \chi^9_{[211]} = \frac{1}{\sqrt{2}}(\bar{g}\,\bar{b}-\bar{b}\,\bar{g}). \tag{26}$$

Then the color wave functions of $QQ-\bar{q}\,\bar{q}$ structure are shown as

$$\psi^{c_1} = \sqrt{\frac{1}{6}}\Big[\chi^1_{[2]}\chi^1_{[22]} - \chi^2_{[2]}\chi^2_{[22]} + \chi^3_{[2]}\chi^3_{[22]} + \chi^4_{[2]}\chi^4_{[22]} - \chi^5_{[2]}\chi^5_{[22]} + \chi^6_{[2]}\chi^6_{[22]}\Big],$$
$$\psi^{c_2} = \sqrt{\frac{1}{3}}\Big[\chi^7_{[11]}\chi^7_{[211]} - \chi^8_{[11]}\chi^8_{[211]} + \chi^9_{[11]}\chi^9_{[211]}\Big]. \tag{27}$$

Finally, we can acquire the total wave functions by substituting the wave functions of the orbital, the spin, the flavor, and the color parts into Eq. (7) according to the definite quantum number of the system.

III. RESULT AND DISCUSSION

In this work, we investigate the double-charm and double-strange tetraquark system $cc\bar{s}\,\bar{s}$ in the framework of QDCSM. Two structures, $Q\bar{q}-Q\bar{q}$ and $QQ-\bar{q}\bar{q}$ structures, as well as the channel coupling of the two configurations are considered. Since we focus on the S-wave states, the orbital angular momentum is set to be zero. The spin quantum number of the $cc\bar{s}\,\bar{s}$ system can be 0, 1, and 2, so the total angular momentum can be $J=0$, 1, and 2 for this system. The isospin of the c or s quark is zero. In this way, the quantum number of the $cc\bar{s}\,\bar{s}$ tetraquark system can be $IJ^P = 00^+$, 01^+, and 02^+. The energy of the $cc\bar{s}\bar{s}$ tetraquark systems for both the $Q\bar{q}-Q\bar{q}$ and $QQ-\bar{q}\bar{q}$ structures, as well as the channel coupling of these two structures, is listed in Table I, where E_{sc} is the energy of every single channel, E_{cc} shows the energy by channel coupling of one certain configuration, and $E_{\rm mix}$ is the lowest energy of the system by coupling all channels of both configurations.

TABLE I. The energies of the $cc\bar{s}\,\bar{s}$ system.

IJ^P	Channel	Threshold	E_{sc}	E_{cc}	$E_{\rm mix}$
00^+	$D_s^+D_s^+$	3936	3942	3942	3939
	$D_s^{*+}D_s^{*+}$	4224	4228		
	$(cc)_{\bar{3}}(\bar{s}\bar{s})_3$		4372	4312	
	$(cc)_{\bar{6}}(\bar{s}\bar{s})_6$		4410		
01^+	$D_s^+D_s^{*+}$	4080	4086	4086	4083
	$(cc)_{\bar{3}}(\bar{s}\bar{s})_3$		4393	4393	
02^+	$D_s^{*+}D_s^{*+}$	4224	4230	4230	4225
	$(cc)_{\bar{3}}(\bar{s}\bar{s})_3$		4422	4422	

Here, we should mention that the definition of different $Q\bar{q}-Q\bar{q}$ channels, like the channels $D_s^+D_s^+$, $D_s^{*+}D_s^{*+}$, and so on, just represents the coupling sequences. In the real $Q\bar{q}-Q\bar{q}$ system, the identical quarks in different clusters will exchange between two clusters due to the antisymmetrization operator. Besides, the introduction of the delocalization parameter in QDCSM also allows the quark to run between two clusters, especially when two clusters are very close. So the $D_s^+D_s^+$ channel does not simply refer to the state composed of two D_s^+'s. Instead, it stands only for the coupling sequence. However, when two clusters are far apart, the exchange interaction between two clusters will approach zero, and the delocalization parameter will be zero, too. Then the $D_s^+D_s^+$ channel in this case really represents the two D_s^+ mesons. For convenience, we use this kind of representation for each $Q\bar{q}-Q\bar{q}$ channel in the following discussions. For the $IJ^P = 00^+$ system, there are four channels, which are $D_s^+D_s^+$, $D_s^{*+}D_s^{*+}$, and two $QQ-\bar{q}\,\bar{q}$ channels with the color configurations $(\bar{3}\times 3)$ and $(\bar{6}\times 6)$. For the $Q\bar{q}-Q\bar{q}$ structure, the energies of both the $D_s^+D_s^+$ and $D_s^{*+}D_s^{*+}$ channels are above the corresponding threshold, which means that neither of them are a bound state. The lowest energy is almost unchanged after the channel-coupling calculation, which means that the effect of the channel coupling cannot help too much to form the bound state. This is mainly due to the large mass gap between the $D_s^+D_s^+$ and $D_s^{*+}D_s^{*+}$ channels. For the $QQ-\bar{q}\bar{q}$ structure, it is obvious that the energies of both channels are much higher than those of the $Q\bar{q}-Q\bar{q}$ structure. Although the energy is pushed down about 60 MeV by coupling these two channels, it is still higher than the $Q\bar{q}-Q\bar{q}$ structure. By coupling all channels of both structures, the lowest energy is still above the threshold of the $D_s^+D_s^+$, which indicates that there is no bound state below the minimum threshold (3936 MeV) for the $IJ^P = 00^+$ system.

For the $IJ^P = 01^+$ system, the threshold of $D_s^+D_s^{*+}$ is 4080 MeV, and the energies of the two structures are 4086 and 4393 MeV, respectively, both of which are higher than

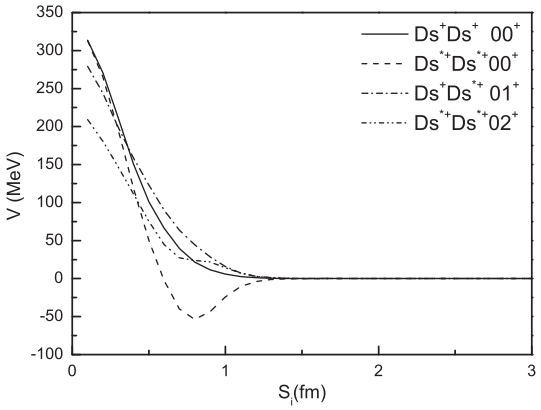

FIG. 1. The effective potentials for the systems with the $c\bar{s} - c\bar{s}$ configuration.

the threshold of $D_s^+ D_s^{*+}$. Then, channel coupling of two structures has been performed and the energy $E_{\mathrm{mix}} = 4083$ MeV is obtained, which is still higher than the threshold. Therefore, no bound state below the threshold (4080 MeV) is obtained for the $IJ^P = 01^+$ system.

For the $IJ^P = 02^+$ system, the case is similar to the one of the $IJ^P = 01^+$ system. The energy of each single channel is above the threshold of the $D_s^{*+} D_s^{*+}$. The channel coupling cannot help too much. So there is no bound state below the threshold (4224 MeV) for the $IJ^P = 02^+$ system, either.

To study the interaction between two clusters, we also carry out an adiabatic calculation of the effective potentials for the $cc\bar{s}\,\bar{s}$ system with two structures, the results of which are shown in Figs. 1 and 2, respectively. For systems with the $c\bar{s} - c\bar{s}$ configuration, it is obvious that the effective potentials of the $IJ^P = 00^+$ $D_s^+ D_s^+$, $IJ^P = 01^+$ $D_s^+ D_s^{*+}$, and $IJ^P = 02^+$ $D_s^{*+} D_s^{*+}$ channels are all repulsive. That is why none of these channels are bound. However, the effective potential of the $IJ^P = 00^+$ $D_s^{*+} D_s^{*+}$ channel is attractive, which indicates that it is possible for this channel to form a bound state or resonance state. Although the bound-state calculation shows that this channel is unbound, it is possible to be a resonance state by channel coupling, which will be discussed later.

For systems with the $cc - \bar{s}\bar{s}$ configuration, the colorful subclusters diquark and antidiquark cannot fall apart directly due to the color confinement, so it is possible for them to be resonance states. From Fig. 2, we can see that the minimum potential of each channel appears at the separation of ~ 0.7 fm, which indicates that two subclusters are not willing to huddle together or fall apart. Besides, the energy of each channel is higher than the corresponding threshold according to Table I, so each channel is possible to be a resonance state.

To find out if there is any genuine resonance state, a stabilization method, also named as a real-scaling method, which has proven to be a valuable tool for estimating the energies of the metastable states of electron-atom, electron-molecule, and atom-diatom complexes [55], is employed here. In this method, with the increase of the distance between two clusters, the continuum state will fall off toward its threshold, while a resonance state will tend to be stable. In this situation, the resonance line acts as an avoid-crossing structure, as shown in Fig. 3. The appearance of the avoid-crossing structure is due to one of the energy of the scattering states getting close to the energy of the genuine resonance with the increasing of the scaling factor, and the coupling will become stronger. The avoid-crossing structure is a general property of interacting two-level systems. If the avoid-crossing structure can repeat with the increasing of the scaling factor, the avoid-crossing structure may be a genuine resonance. This method has been successfully applied to pentaquark systems [56,57], fully heavy tetraquark systems [58], and $c\bar{c}s\bar{s}$ tetraquark systems [13]. A similar idea was also applied to probe the Δ resonance properties from the finite-volume energy spectrum [59]. In this work, the distance between two clusters is labeled as S_i, and the largest one is S_m. Here, we calculate the energy eigenvalues of the $cc\bar{s}\,\bar{s}$ tetraquark systems by taking the value of the distance (S_m) between two clusters

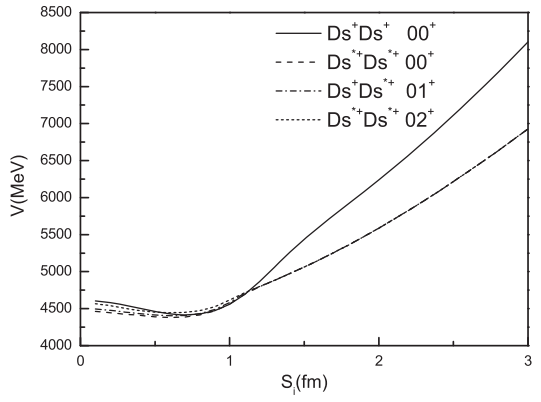

FIG. 2. The effective potentials for the systems with the $cc - \bar{s}\bar{s}$ configuration.

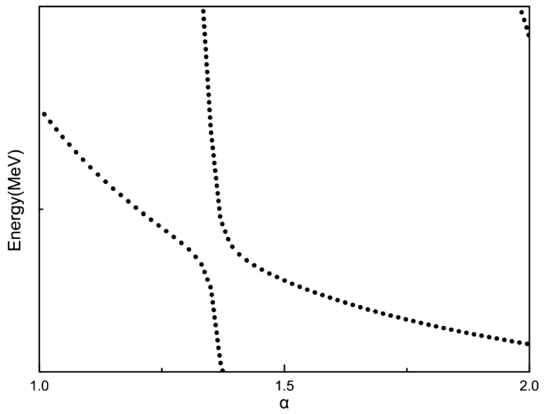

FIG. 3. The shape of the resonance in the real-scaling method. Taken from Ref. [55].

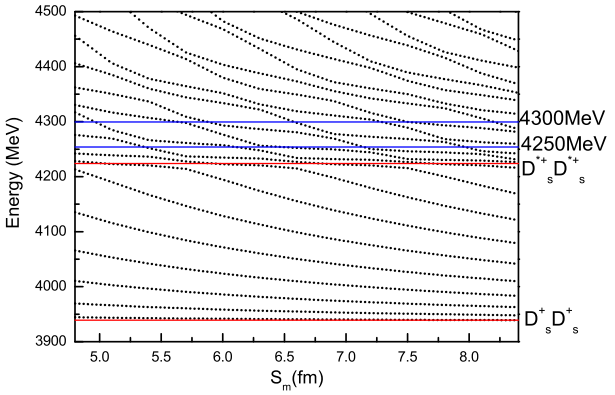

FIG. 4. The stabilization plots of the energies of the $cc\bar{s}\,\bar{s}$ system with $IJ^P = 00^+$.

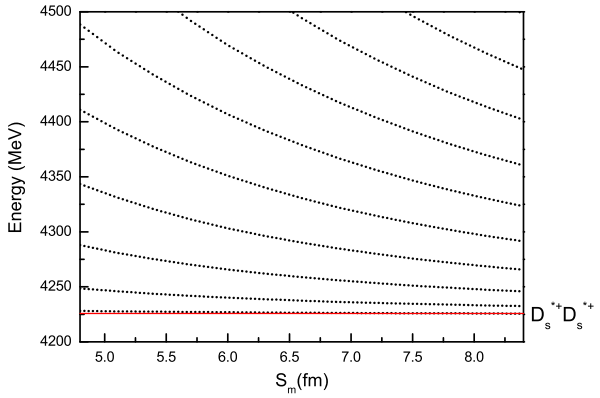

FIG. 7. The stabilization plots of the energies of the $cc\bar{s}\,\bar{s}$ with $IJ^P = 02^+$.

from 4.7 to 8.4 fm to see if there is any resonance state. The results of the $cc\bar{s}\,\bar{s}$ tetraquark systems with $IJ^P = 00^+$, 01^+, and 02^+ are shown in Figs. 4–7, respectively.

For the $cc\bar{s}\,\bar{s}$ system with $IJ^P = 00^+$ in Fig. 4, it is clear that the first two horizontal lines locate at the corresponding physical threshold of two channels $D_s^+ D_s^+$ and $D_s^{*+} D_s^{*+}$. We mark them with red lines. The genuine resonances, which appear as the avoid-crossing structure, are marked with blue lines. To better distinguish the resonant states, we observe the resonant states in the energy range from 4150 to 4500 MeV, which are shown in Fig. 5. In Fig. 5, three avoid-crossing structures appear around the energy of 4250 MeV, which indicates the existence of a resonance state. We mark the avoid-crossing structure with a red circle. Besides, there are two avoid-crossing structures around the energy 4300 MeV, which corresponds to another resonance state.

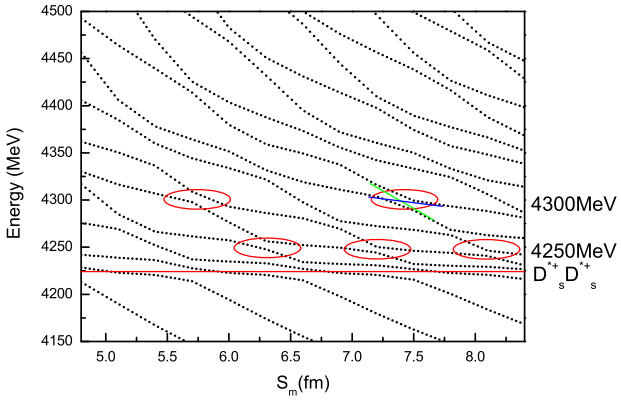

FIG. 5. The stabilization plots of the energies of the $cc\bar{s}\,\bar{s}$ system with $IJ^P = 00^+$ in the energy range from 4150 to 4500 MeV.

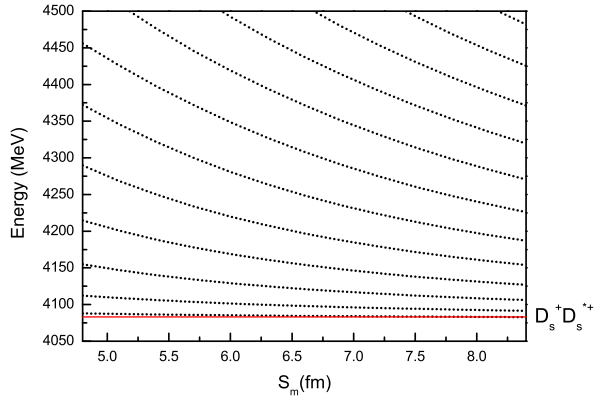

FIG. 6. The stabilization plots of the energies of the $cc\bar{s}\,\bar{s}$ system with $IJ^P = 01^+$.

To calculate the decay width of the resonance state, we use the formula in Ref. [55]:

$$\Gamma = 4V(S_i)\frac{\sqrt{|k_r \times k_c|}}{|k_r - k_c|}, \tag{28}$$

where the $V(S_i)$ is the minimal energy difference between the resonance state and the scattering state. Actually, either of these two states can be coupled by many channels. So Eq. (28) can be viewed as calculating the total widths of resonance states. Take the work of Ref. [57], for example; the $C = 1$ and 2 are the contributions from "continuum" (scattering) channels, and $C = 3$ and 4 are the connected Jacobi coordinate systems, which are the closed channels. In Fig. 5(a) in Ref. [57], only scattering configurations of $C = 1$ and 2 are included, so there is no resonance state; while in Fig. 5(b) in Ref. [57], full configurations of $C = 1$–4 are considered, which include two scattering channels and two closed channels, and finally one resonance state is obtained around 4690 MeV. The decay width of this resonance state calculated by Eq. (9) in Ref. [55] is the total width of the state decaying to two scattering channels. We have checked the validity of the approach in the multichannel problem, and the results show that the generalization from a two-channel problem to a multichannel problem is reasonable. For example, we calculated the partial decay width of the P_{cs} state to each open channel

and added them to obtain the total width [60]. On the other hand, we directly coupled all open and closed channels to obtain the total width. Finally, we found that the decay widths obtained by these two methods were basically the same.

In Fig. 5, one can extract the total decay widths from every avoid-crossing structure. However, the larger the space, the more stable the result, so we generally choose to calculate the decay width in a larger space. k_r and k_c in Eq. (28) stand for the slope of the resonance state and the scattering state, respectively. In Fig. 5, taking the resonance state of 4300 MeV, for example, the blue line represents the slope k_r, which is about -14.7, and the green line stands for the slope k_c, which is about -90. Substituting these values into Eq. (28), we obtain the width of the resonance state 4300 MeV, which is about 19 MeV. For the resonance state of 4250 MeV, the decay width is 6 MeV.

Besides, to investigate the structure of these two resonance states, we also calculate the component of each channel for these two resonance states, as well as the root mean square radius for them. Actually, the wave function of the resonance state is not a square-integrable function, but the one of the bound state is a square-integrable function. So we can calculate the root mean square radius by using the wave function of the bound state, which is obtained without coupling to the open channels. The bound state will decay to the corresponding open channels and becomes a resonance state. For the resonance state with the mass of 4250 MeV, the proportions of the channels $D_s^+D_s^+$ and $D_s^{*+}D_s^{*+}$ are about 10% and 80%, respectively, while the one of the $cc-\bar{s}\bar{s}$ channels is about 10%. This is possible, because the attractive potential of the $D_s^{*+}D_s^{*+}$ channel shown in Fig. 1 provides the mechanism for forming a resonance state. When we carry out the three-channel coupling calculation of $D_s^{*+}D_s^{*+}$ and two $cc-\bar{s}\,\bar{s}$ channels, a bound state is obtained with the $D_s^{*+}D_s^{*+}$ channel as the main component. So we calculate the root mean square radius by using the wave function of this three-channel coupling situation. The root mean square radius of this resonance is around 0.48 fm, which indicates that two clusters are not willing to huddle together or to separate too far. So this resonance state is more inclined to be the compact structure rather than the molecular structure, though the main component is the $D_s^+D_s^+$ and $D_s^{*+}D_s^{*+}$ channels. This is understandable in QDCSM. Since the quark delocalization and color screening in QDCSM include the effective description of hidden-color channel coupling [61], it is possible for the $Q\bar{q}-Q\bar{q}$ structure to form color structure resonance states, which is not a pure molecular state.

For the resonance state with the mass of 4300 MeV, the proportion of the channels $D_s^+D_s^+$ and $D_s^{*+}D_s^{*+}$ is about 20% and 20%, respectively, while the one of the $cc-\bar{s}\bar{s}$ structure is about 60%. So the root mean square radius of this resonance is calculated by using the wave function of the two-channel coupling of the $cc-\bar{s}\bar{s}$ structure, and it is also around 0.48 fm. It means that this resonance state is also more likely to be a compact state.

The results of the $cc\bar{s}\,\bar{s}$ systems with $IJ^P=01^+$ and 02^+ are shown in Figs. 6 and 7, respectively. The first horizontal line in the two figures represents the threshold of the $D_s^+D_s^{*+}$ and $D_s^{*+}D_s^{*+}$, respectively. It is obvious that, with the increase of the distance between two clusters, the energy of the continuum state falls off toward its threshold. So there is no resonance state for the $cc\bar{s}\,\bar{s}$ systems with $IJ^P=01^+$ and 02^+.

IV. SUMMARY

In this work, we systematically investigate the low-lying double-charm and double-strange tetraquark systems $cc\bar{s}\,\bar{s}$ in the framework of the QDCSM. Two structures, $Q\bar{q}-Q\bar{q}$ and $QQ-\bar{q}\bar{q}$, as well as the coupling of these two configurations are considered. The dynamical bound-state calculation is carried out to search for any bound state in the $cc\bar{s}\bar{s}$ systems. Meanwhile, an adiabatic calculation of the effective potentials is added to study the interactions of the systems, and a stabilization calculation is carried out to find any resonance state.

The bound-state calculation shows that there is no bound state lower than the lowest threshold for the $cc\bar{s}\,\bar{s}$ system in QDCSM. However, two resonance states with $IJ^P=00^+$ are obtained, one with a mass and width around 4250 and 6 MeV, respectively, and another one with a mass and width around 4300 and 19 MeV, respectively. The root mean square radius of these two resonance states indicates that both of these states are more inclined to be compact resonance states. Besides, our results show that the coupling calculation is indispensable to explore the resonance states. In the work of the chiral quark model [46], there was no bound state for the $cc\bar{s}\bar{s}$ system, either. However, several resonance states were obtained for $cc\bar{s}\bar{s}$ tetraquarks, which were one $IJ^P=00^+$ state with a resonance mass around 4.9 GeV and three $IJ^P=02^+$ states with a resonance mass around 4.8 GeV. Besides, the work in Ref. [47] also studied the state with $C=2$, $S=2$, $I=0$, and $J=0$, 2, and no state was obtained in this sector. However, only the $D_s^*D_s^*$ channel was studied there. The coupling with other channels is worthy of consideration to find some resonance states.

Besides, although no significant signals were observed in the present experiment at the Belle Collaboration [45], there are still some structures around 4.3 GeV in the distributions of $M_{D_s^+D_s^+}$ and $M_{D_s^{*+}D_s^{*+}}$. We suggest that the experiment check with a larger amount of data in the future.

ACKNOWLEDGMENTS

This work is supported partly by the National Natural Science Foundation of China under Contracts No. 11675 080, No. 11775118, and No. 11535005.

[1] T. Aaltonen *et al.* (CDF Collaboration), Phys. Rev. Lett. **102**, 242002 (2009).
[2] C. P. Shen *et al.* (Belle Collaboration), Phys. Rev. Lett. **104**, 112004 (2010).
[3] S. Chatrchyan *et al.* (CMS Collaboration), Phys. Lett. B **734**, 261 (2014).
[4] V. M. Abazov *et al.* (D0 Collaboration), Phys. Rev. D **89**, 012004 (2014).
[5] J. P. Lees *et al.* (*BABAR* Collaboration), Phys. Rev. D **91**, 012003 (2015).
[6] R. Aaij *et al.* (LHCb Collaboration), Phys. Rev. D **85**, 091103 (2012).
[7] R. Aaij *et al.* (LHCb Collaboration), Phys. Rev. Lett. **118**, 022003 (2017).
[8] R. Aaij *et al.* (LHCb Collaboration), Phys. Rev. D **95**, 012002 (2017).
[9] T. Aaltonen *et al.* (CDF Collaboration), Phys. Lett. A **32**, 1750139 (2017).
[10] R. Aaij *et al.* (LHCb Collaboration), Phys. Rev. Lett. **125**, 242001 (2020).
[11] R. Aaij *et al.* (LHCb Collaboration), Phys. Rev. D **102**, 112003 (2020).
[12] R. Aaij *et al.* (LHCb Collaboration), Phys. Rev. Lett. **127**, 082001 (2021).
[13] X. J. Liu, H. X. Huang, J. L. Ping, D. Y. Chen, and X. M. Zhu, Eur. Phys. J. C **81**, 950 (2021).
[14] Y. F. Yang and J. L. Ping, Phys. Rev. D **99**, 094032 (2019).
[15] H. X. Chen, E. L. Cui, W. Chen, X. Liu, and S. L. Zhu, Eur. Phys. J. C **77**, 160 (2017).
[16] J. Wu, Y. R. Liu, K. Chen, X. Liu, and S. L. Zhu, Phys. Rev. D **94**, 094031 (2016).
[17] Z. G. Wang, Eur. Phys. J. C **77**, 78 (2017).
[18] Q. F. Lv and Y. B. Dong, Phys. Rev. D **94**, 074007 (2016).
[19] P. G. Ortega, J. Segovia, D. R. Entem, and F. Fernandez, Phys. Rev. D **94**, 114018 (2016).
[20] L. Maiani, A. D. Polosa, and V. Riquer, Phys. Rev. D **94**, 054026 (2016).
[21] C. R. Deng, J. L. Ping, H. X. Huang, and F. Wang, Phys. Rev. D **98**, 014026 (2018).
[22] E. S. Swanson, Phys. Rev. D **91**, 034009 (2015).
[23] M. Ablikim *et al.* (BESIII Collaboration), Phys. Rev. Lett. **126**, 102001 (2021).
[24] X. Jin, Y. H. Wu, X. J. Liu, H. X. Huang, J. L. Ping, and B. Zhong, Eur. Phys. J. C **81**, 1108 (2021).
[25] Z. F. Sun and C. W. Xiao, arXiv:2011.09404.
[26] X. Cao, J. P. Dai, and Z. Yang, Eur. Phys. J. C **81**, 184 (2021).
[27] M. C. Du, Q. Wang, and Q. Zhao, arXiv:2011.09225.
[28] J. Z. Wang, Q. S. Zhou, X. Liu, and T. Matsuki, Eur. Phys. J. C **81**, 51 (2021).
[29] Z. Yang, X. Cao, F. K. Guo, J. Nieves, and M. P. Valderrama, Phys. Rev. D **103**, 074029 (2021).
[30] K. Azizi and N. Er, Eur. Phys. J. C **81**, 61 (2021).
[31] B. Wang, L. Meng, and S. L. Zhu, Phys. Rev. D **103**, L021501 (2021).
[32] Y. A. Simonov, J. High Energy Phys. 04 (2021) 051.
[33] Z. G. Wang, Chin. Phys. C **45**, 073107 (2021).
[34] R. Chen and Q. Huang, Phys. Rev. D **103**, 034008 (2021).
[35] L. Meng, B. Wang, and S. L. Zhu, Phys. Rev. D **102**, 111502 (2020).
[36] B. D. Wan and C. F. Qiao, Nucl. Phys. **B968**, 115450 (2021).
[37] G. C. Rossi and G. Veneziano, Nucl. Part. Phys. Proc. **312**, 140 (2021).
[38] M. J. Yan, F. Z. Peng, M. Sanchez Sanchez, and M. Pavon Valderrama, Phys. Rev. D **104**, 114025 (2021).
[39] Q. N. Wang, W. Chen, and H. X. Chen, Chin. Phys. C **45**, 093102 (2021).
[40] P. G. Ortega, D. R. Entem, and F. Fernandez, Phys. Lett. B **818**, 136382 (2021).
[41] J. F. Giron, R. F. Lebed, and S. R. Martinez, Phys. Rev. D **104**, 054001 (2021).
[42] L. Meng, B. Wang, G. J. Wang, and S. L. Zhu, Sci. Bull. **66**, 2065 (2021).
[43] H. X. Chen, Phys. Rev. D **105**, 094003 (2022).
[44] P. P. Shi, F. Huang, and W. L. Wang, Phys. Rev. D **103**, 094038 (2021).
[45] X. Y. Gao *et al.* (Belle Collaboration), Phys. Rev. D **105**, 032002 (2022).
[46] G. Yang, J. L. Ping, and J. Segovia, Phys. Rev. D **102**, 054023 (2020).
[47] R. Molina, T. Branz, and E. Oset, Phys. Rev. D **82**, 014010 (2010).
[48] F. Wang, G. H. Wu, L. Jian, and T. Goldman, Phys. Rev. Lett. **69**, 2901 (1992).
[49] P. A. M. Guichon, J. R. Stone, and A. W. Thomas, Prog. Part. Nucl. Phys. **100**, 262 (2018).
[50] J. L. Ping, H. X. Huang, H. R. Pang, F. Wang, and C. W. Wong, Phys. Rev. C **79**, 024001 (2009).
[51] H. X. Huang, J. L. Ping, and F. Wang, Phys. Rev. C **92**, 065202 (2015).
[52] H. X. Huang, C. R. Deng, J. L. Ping, and Fan Wang, Eur. Phys. J. C **76**, 624 (2016).
[53] H. X. Huang and J. L. Ping, Phys. Rev. D **99**, 014010 (2019).
[54] M. Kamimura, Prog. Theor. Phys. Suppl. **62**, 236 (1977).
[55] J. Simon, J. Chem. Phys. **75**, 2465 (1981).
[56] E. Hiyama, M. Kamimura, A. Hosaka, H. Toki, and M. Yahiro, Phys. Lett. B **633**, 237 (2006).
[57] E. Hiyama, A. Hosaka, M. Oka, and J. M. Richard, Phys. Rev. C **98**, 045208 (2018).
[58] X. Jin, Y. Xue, H. Huang, and J. Ping, Eur. Phys. J. C **80**, 1083 (2020).
[59] V. Bernard, M. Lage, U. G. Meissner, and A. Rusetsky, J. High Energy Phys. 08 (2008) 024.
[60] X. H. Hu and J. L. Ping, Eur. Phys. J. C **82**, 118 (2022).
[61] H. X. Huang, P. Xu, J. L. Ping, and F. Wang, Phys. Rev. C **84**, 064001 (2011).